Ultrafast laser writing of arbitrary long low-loss waveguides in optical fibers

Léo Colliard, Guillaume Bilodeau, Tommy Boilard, Jerome Lapointe, Réal Vallée, Martin Bernier, Matthieu Bellec

Optics Letters

Ultrafast laser writing of arbitrary long low-loss waveguides in optical fibers

Léo Colliard,[1,2] Guillaume Bilodeau,[1] Tommy Boilard,[1] Jerome Lapointe,[1] Réal Vallée,[1] Martin Bernier,[1] and Matthieu Bellec[1,2,3,*]

[1]Centre d'optique, photonique et laser (COPL), 2375 rue de la Terrasse, Université Laval, Québec G1V 0A6, Canada
[2]Université Côte d'Azur, CNRS, INPHYNI, France
[3]Université de Bordeaux, CNRS, CEA, CELIA, UMR 5107, F-33405, Talence, France
*Corresponding author: matthieu.bellec@inphyni.cnrs.fr

Received 14 October 2022; revised 1 November 2022; accepted 6 November 2022; posted 7 November 2022; published 29 November 2022

We propose an innovative femtosecond laser writing approach, based on a reel-to-reel configuration, allowing the fabrication of arbitrary long optical waveguides in coreless optical fibers directly through the coating. We report few meters long waveguides operating in the near-infrared (near-IR) with propagation losses as low as 0.055 ± 0.004 dB/cm at 700 nm. The refractive index distribution is shown to be homogeneous with a quasi-circular cross section, its contrast being controllable via the writing velocity. Our work paves the way for the direct fabrication of complex arrangements of cores in standard and exotic optical fibers.

https://doi.org/10.1364/OL.478386

Direct laser writing (DLW) is a mature technology that allows the fabrication of complex three-dimensional (3D) low-loss photonic circuits integrated in glass chips [1–3]. During the last decade, many applications of DLW have emerged such as quantum calculation and sources [4–6], analog simulators [7–9], and sensing devices [10–12], to cite a few. This method consists of tightly focusing an ultrashort intense infrared (IR) laser beam inside a transparent glass sample. Consequently, a nonlinear process induces, at the focal point, a slight microscale modification of the refractive index. By moving the sample, various advanced photonic components such as directional couplers, wavelength division multiplexers, interferometers, gratings, or resonators can be directly integrated in the bulk. Nowadays, advanced beam shaping techniques are commonly used to optimize the energy deposition during the laser–matter interaction allowing the improvement of device performances [13,14]. Beyond its 3D capabilities, the DLW technique also offers a great versatility in terms of materials that can be processed. Glasses can be specifically designed to make the photonic circuits operating at specific wavelengths ranging from the visible to the mid-IR [15].

Although most of the attention has focused on bulk samples, DLW has been recently employed for optical fibers structuring (see, e.g., a recent review [16]). The most common laser-written components are fiber Bragg gratings (FBG) that are now routinely fabricated, directly through the coating, via different methods (e.g., phase mask [17,18], point-by-point [19,20]) for sensing and lasing applications. Beyond FBGs, optical fibers can also be functionalized with laser-inscribed waveguides and microfluidic circuits [16,21–24], giving rise to the so-called lab-in-fibers (LIF) [25]. The current DLW technology restricts the size of the fabricated structures to a few 10s of centimeters due to the limited translation stage range. Moreover, without any additional beam shaping technique [26,27], the waveguide shapes are generally inhomogeneous and highly elongated [22,24], mainly due to spherical aberrations and filamentation effects. To go one step further in the LIF development and bridge the gap between centimeter-long complex structures and kilometer-long ones limited to basic architectures, on-demand complex arrangements of high-quality waveguides at the intermediate meter scale are nowadays a crucial need.

To overcome these limitations, here we exploit a very promising approach, based on a reel-to-reel (R2R) configuration, recently proposed to enhance the scattering properties of optical fibers for distributed sensing applications [28–31]. Using a phase mask technique, we report, for the first time to our knowledge, the fabrication in coreless silica fibers, directly through the polymer coating, of low-loss single mode waveguides of few meter-long operating in the near-IR range. We observe a homogeneous refractive index distribution with a quasi-circular cross section. The index contrast can be tuned by changing the writing velocity. We characterize the modal properties and propagation losses of the waveguides and point out the mechanical limits of our system. Our work paves the way to the direct fabrication of complex arrangements of cores in standard and exotic optical fibers, ultimately integrated in a fiber draw tower [32,33]. Figure 1(a) shows a sketch of the proposed R2R-DLW technique. Via a set of rotating spools and pulleys, a coreless silica fiber (home drawn from a homogeneous high purity fused silica preform Hereaus F300, n_{core} = 1.46, and surrounding by a polyacrylate coating, n_{coat} = 1.54) is translated at constant velocity v, along the z axis, in the path of a tightly focused femtosecond laser beam emitting high-energy 35 fs pulses at 800 nm, and 1 kHz repetition rate (Coherent, Astrella). The details of the focusing stage, which consists of an acylindrical lens (Thorlabs, AYL108-B, 8 mm focal length) and a phase mask (1060.3 nm pitch) positioned 80 µm in front of the fiber coating, are presented in Figs. 1(b) and 1(c). The incoming Gaussian beam

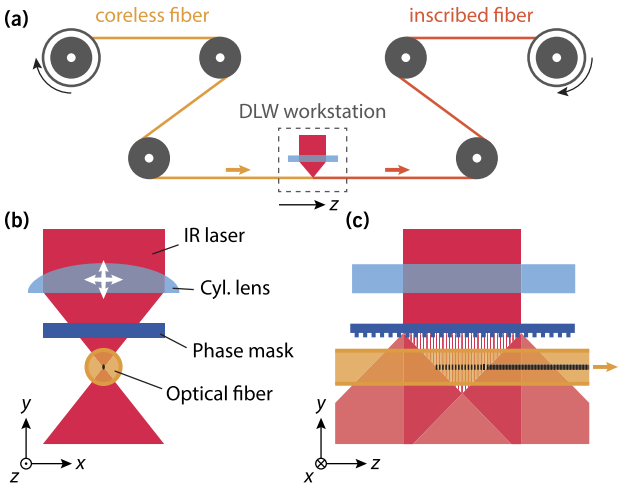

Fig. 1. (a) Simplified sketch of the reel-to-reel direct-laser-writing experimental setup. (b),(c) Details of the focusing system. An IR femtosecond laser is focused in the center of the coreless optical fiber via a cylindrical lens, directly through the coating. A phase mask allows to generate an interference pattern in the (x, y) plane. The translation of the fiber along z creates a smooth waveguide. The lens can be scanned in the x and y directions to finely adjust the waveguide cross section.

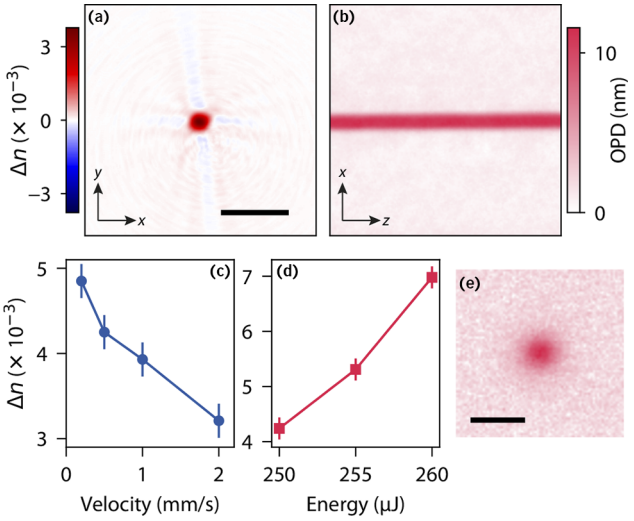

Fig. 2. (a) Transverse refractive index distribution of a DLW waveguide (250 μJ, 1 mm/s). The scale bar is 10 μm. (b) Longitudinal distribution of the optical path difference. Same scale as panel (a). (c),(d) Maximum refractive index values versus (c) writing velocities at $E = 250$ μJ and (d) energy at $v = 0.5$ mm/s. (e) Intensity of the mode at 1100 nm imaged at the output of a 17 cm long sample. The scale bar is 5 μm.

diameter is 11 mm at $1/e^2$. The focal zone consists of a Gaussian-apodized sinusoidal pattern along z with 530 nm period [dotted black pattern in Fig. 1(c)] and a $\sim 2\ \mu m \times 1\ \mu m$ cross section in the (x, y) plane [black spot in Fig. 1(b)]. The lens can be scanned in the x and y directions, via a piezo motor (PI, P-611XZ) to optimize the waveguide cross section. To obtain a quasi-circular refractive index distribution, the lens is moved along the x axis at 4 Hz over ±1.5 μm. When used with a fixed optical fiber, this configuration is typically employed to write efficient FBGs (see our previous works for more experimental details [17]). With this specific phase mask, the Bragg wavelength is expected to be near 1537 nm. Here, while the acylindrical lens reduces the spherical aberrations in the (x, y) plane [34], the phase mask essentially stabilizes the multi-filamentation process that might occur in the (y, z) plane [35]. The writing beam is thus distributed over 1000s of periodically arranged spots which allows us to parallelize and speed up significantly the waveguide processing up to millimeters per second, while usually limited to a few micrometers per second in fused silica with such low repetition rate laser system [36], although some progress has been reported recently [37]. The longitudinal translation of the fiber, at constant v of the order of few millimeters per second, is ensured by a dedicated mechanical setup which includes a tension controller. In the present experiments, the longitudinal tension applied to the fiber is tuned to 4 N. The continuous motion of the fiber smooths the grating pattern out and ensures a homogeneous, arbitrary long, refractive index modification [see the black line in Fig. 1(c)]. The optical fiber is imaged with a CMOS camera (IDS, UI-2230SE) mounted with a microscope objective (Mitutoyo, 10×, NA = 0.28). The whole setup is initially aligned by visualizing the luminescence induced when the writing laser interact with the core of a standard Ge-doped SMF-28 fiber [38]. After swapping it with the fiber of interest, the same imaging setup is used to monitor the plasma visible emission occurring during the laser–matter interaction [2].

The refractive index transverse distribution of a 10 cm-long waveguide inscribed in a F300 coreless optical fiber at 250 μJ and $v = 1$ mm/s is depicted in Fig. 2(a). The intensity of each spot of the beam is estimated to $\sim 2 \times 10^{14}$ W/cm^2. The measurement is performed by an interferometric fiber analyzer (Interfiber Analysis, IFA-100). In contrast with results reported for a standard focusing setup [22,24], we observe a rather symmetric and homogeneous Gaussian distribution with horizontal (respectively, vertical) full width at half maximum (FWHM) of 2.5 ± 0.1 μm (respectively, 2.1 ± 0.1 μm), i.e., with an aspect ratio of 0.84. The maximum refractive index value for this condition is $\Delta n = 3.8 \pm 0.2 \times 10^{-3}$. Note that the distribution has been averaged over different positions along the laser-written core and for different inscription runs. Figure 2(b) depicts the longitudinal distribution of the optical path difference (OPD) measured with a wavefront sensor (Phasics, SID4) attached to an optical microscope. At this scale, the OPD is also very homogeneous. From the maximum value of the OPD and e the thickness of the waveguide estimated from Fig. 2(a), we obtain $\Delta n = \mathrm{OPD}/e \sim 4 \times 10^{-3}$ [39]. The writing velocity has then been varied from 0.1 to 2 mm/s. As shown in Fig. 2(c), Δn decreases with the writing velocity, from 4.9 to 3.2×10^{-3}, as expected. At fixed velocity, the refractive index also increases with the pulse energy as shown in Fig. 2(d). Note that the damage threshold is very close to 260 μJ, the nominal value is thus tuned to 250 μJ. Figure 2(e) shows the mode intensity, excited at 1100 nm and imaged at the exit face of a 17 cm-long sample written under the same conditions. We clearly observe a single mode operation. Note that the cutoff wavelength is estimated numerically (Lumerical, Ansys), from the refractive index distribution in Fig. 2(a), to 385 nm. Note that we did not manage to inscribe any waveguides without the phase mask, thus confirming its decisive role.

Before describing the propagation losses of the inscribed structures, it is worth investigating the mechanical stability and

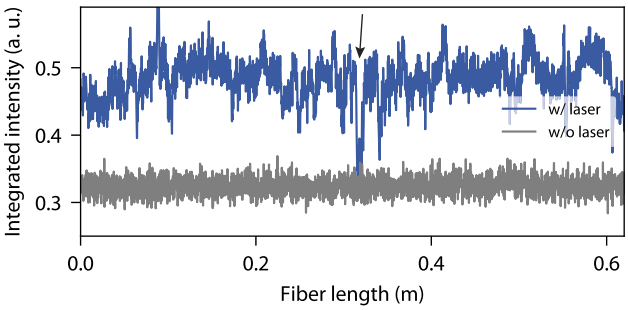

Fig. 3. Integrated intensity of the laser-induced plasma recorded during the fabrication of a 600 mm-long waveguide at 1 mm/s (blue). Same signal when the writing laser is off (gray).

the limitations of the proposed R2R-DLW system. We first measure the central transverse coordinates of various waveguides fabricated in similar conditions. We obtain a scattered distribution around the fiber center with a standard deviation of 3.5 μm. To get more insight on the mechanical stability of the system, we monitor the transverse position of the fiber during the writing process. At a large longitudinal scale, the typical fluctuations are ±2 μm in accordance with the standard deviation of the waveguide centers. These random instabilities likely come from the fiber slippage in the V-groove of the pulleys and from the mechanical noise of the motor managing the fiber tension. In order to improve the precision of our system, a method for accurate auto-positioning of the fiber, via an image processing similar to Ref. [40], is envisaged as a short-term solution.

In addition, Fig. 3 presents the signal emitted from the laser-induced plasma generated during the writing process (blue curve) in the same conditions. Each point of the signal is collected by integrating, for each frame, the intensity of the (y, z) image over a region of interest (ROI) which corresponds to the plasma emission. The ROI is a large enough box (i.e., 0.8 mm × 20 μm) centered along the x-axis of the fiber. The background noise level (gray signal) is obtained by repeating the experiment and the subsequent image processing (same ROI) without the writing laser. Since the plasma signal is supposed to be maximum when the laser is perfectly focused at the center of the fiber, the instabilities likely originate from the fiber displacements discussed previously. In addition, some sharp dips can be observed (see black arrow) indicating that the laser beam was not optimally delivered to the optical fiber and, consequently, that the quality of the waveguide might be degraded locally thus inducing additional losses. This might come from dust at the fiber surface or defects in the (homemade) polymer coating. However, this is mitigated by the elongated shape of the writing beam that tends to smooth the refractive index modification. Indeed, only a few of them showed a slight longitudinal variation of the OPD within 10 μm of the length.

Finally, to measure the propagation losses, a cutback method is implemented on a 3.7 m long waveguide, fabricated at 250 μJ and 1 mm/s. The spectral transmission is measured from 700 to 1100 nm for various waveguide lengths by coupling a supercontinuum source (Koheras, SuperK Power) to the waveguide input with an aspheric lens (New Focus, 5726-B) and by recording the transmitted signal with an optical spectrum analyzer (OSA) (Yokogawa, AQ6373B). Three spectra are depicted in Fig. 4(a) for short, intermediate, and long samples. The signal is quite sensitive to the microbends present in the bare fiber adaptor connected to the OSA, so each measurement was averaged over

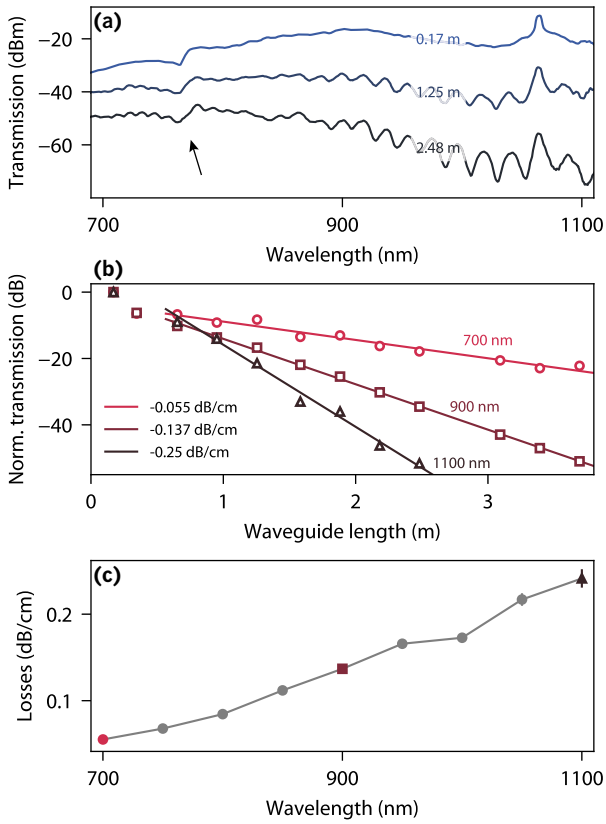

Fig. 4. (a) Transmission spectra for different waveguide lengths. (b) Normalized transmission versus waveguide length at 700 nm (circle), 900 nm (square), and 1100 nm (triangle). Error bars are in the markers. Solid lines are linear fits that give losses of 0.055 ± 0.004, 0.137 ± 0.002, and 0.25 ± 0.01 dB/cm, at 700, 900, and 1100 nm, respectively. (c) Propagation losses versus input wavelength obtained from linear fits. Error bars are contained in the markers if not visible.

multiple configurations (i.e., removing the fiber from the adaptor and plugging it back to the OSA). During the measurements, the power fluctuations of the source were negligible. The typical error is ±1 dB. Note that the black arrow indicates a slight dip at 768 nm which corresponds to the second order of the FBG whose reminiscent response is expected at 1537 nm.

Figure 4(b) shows the transmission, normalized to the maximum value, versus the waveguide length at 700, 900, and 1100 nm. Via a linear fitting procedure (solid lines), we extract propagation losses of 0.055 ± 0.004, 0.137 ± 0.002, and 0.25 ± 0.01 dB/cm, respectively. Note that we exclude from the fits the samples shorter than 50 cm. Indeed, they present larger losses likely coming from mode filtering mechanism occurring early in the propagation. This is currently under investigation. We repeat the procedure for intermediate wavelengths [see Fig. 4(c)] and see that the propagation losses monotonically decreases with the wavelength. As expected, the mode is better confined as one approaches the cutoff and is thus less affected by possible irregularities at the core-cladding interface. This would clearly be pointing to the main source of losses in such photo-inscribed waveguides. It is worth noting that despite the limited mechanical stability of the setup and the fact that fused silica glasses (and especially F300) are known to be hardly laser-processable, the waveguiding properties presented here are rather good with

record low losses at 700 nm. By optimizing the R2R-DLW setup and choosing more appropriate glass composition (such as BGG glasses [15]), there is room to improve further the waveguide quality, increase the cutoff wavelength, and make it operate efficiently in the telecom range.

In conclusion, an innovative reel-to-reel direct-laser-writing setup has been successfully implemented to inscribe arbitrary long and low-loss waveguides in a coreless fused silica optical fiber, directly through the coating. Up to 3.7 m low-loss single-mode waveguide operating in the near-IR have been reported for the first time. The refractive index is homogeneous and its value can be adjusted by varying the writing velocity. The propagation losses have been measured in a repeatable way. In the near future, we aim at optimizing the writing setup and glass composition to further improve the waveguide properties in the telecom and mid-IR range. Our results pave the way toward the realization of more complex photonic cores arrangements in exotic optical fibers (in which core/cladding structures are hard to fabricate) with a potential implementation directly in a fiber draw tower [32,33]. Another promising perspective is related to the inherent weak continuous distribution of FBGs that could be useful for the implementation of random fiber lasers or distributed sensors [29,41–43].

Funding. Horizon 2020 Framework Programme (823941); Agence Nationale de la Recherche (ANR-15-IDEX-01); Canada Foundation for Innovation (5180); Fonds de recherche du Québec – Nature et technologies (CRDPJ-543631-19, IRCPJ469414-18, RGPIN-2016-05877); Canada First Research Excellence Fund (Sentinel North program).

Acknowledgments. The authors would like to thank B. Méthot and S. Gagnon for technical assistance and L. Canioni for fruitful discussions.

Disclosures. The authors declare no conflicts of interest.

Data availability. Data underlying the results presented in this paper are not publicly available at this time but may be obtained from the authors upon reasonable request.

REFERENCES

1. K. M. Davis, K. Miura, N. Sugimoto, and K. Hirao, Opt. Lett. **21**, 1729 (1996).
2. R. R. Gattass and E. Mazur, Nat. Photonics **2**, 219 (2008).
3. D. Tan, Z. Wang, B. Xu, and J. Qiu, Adv. Photonics **3**, 024002 (2021).
4. A. Crespi, R. Osellame, R. Ramponi, D. J. Brod, E. F. Galv ao, N. Spagnolo, C. Vitelli, E. Maiorino, P. Mataloni, and F. Sciarrino, Nat. Photonics **7**, 545 (2013).
5. R.-J. Ren, J. Gao, W.-H. Zhou, Z.-Q. Jiao, L.-F. Qiao, X.-W. Wang, and X.-M. Jin, Phys. Rev. Appl. **16**, 054026 (2021).
6. G. Corrielli, A. Crespi, and R. Osellame, Nanophotonics **10**, 3789 (2021).
7. A. Crespi, R. Osellame, R. Ramponi, V. Giovannetti, R. Fazio, L. Sansoni, F. De Nicola, F. Sciarrino, and P. Mataloni, Nat. Photonics **7**, 322 (2013).
8. M. Bellec, C. Michel, H. Zhang, S. Tzortzakis, and P. Delplace, EPL **119**, 14003 (2017).
9. M. Kremer, L. J. Maczewsky, M. Heinrich, and A. Szameit, Opt. Mater. Express **11**, 1014 (2021).
10. J. Lapointe, M. Gagné, M.-J. Li, and R. Kashyap, Opt. Express **22**, 15473 (2014).
11. A. Crespi, M. Lobino, J. C. F. Matthews, A. Politi, C. R. Neal, R. Ramponi, R. Osellame, and J. L. O'Brien, Appl. Phys. Lett. **100**, 233704 (2012).
12. A. A. Khalil, P. Lalanne, J.-P. Bérubé, Y. Petit, R. Vallée, and L. Canioni, Opt. Express **27**, 31130 (2019).
13. P. S. Salter and M. J. Booth, Light: Sci. Appl. **8**, 110 (2019).
14. J. Lapointe, J.-P. Bérubé, A. Dupont, M. Bellec, and R. Vallée, Appl. Opt. **61**, 2333 (2022).
15. A. L. Camus, Y. Petit, J.-P. Bérubé, M. Bellec, L. Canioni, and R. Vallée, Opt. Express **29**, 8531 (2021).
16. J. Zhao, Y. Zhao, Y. Peng, R. qing Lv, and Q. Zhao, Opt. Laser Technol. **146**, 107473 (2022).
17. J. Habel, T. Boilard, J.-S. Frenière, F. Trépanier, and M. Bernier, Sensors **17**, 2519 (2017).
18. S. J. Mihailov, C. Hnatovsky, N. Abdukerim, R. B. Walker, P. Lu, Y. Xu, X. Bao, H. Ding, M. De Silva, D. Coulas, and D. Grobnic, Sensors **21**, 1447 (2021).
19. A. Martinez, I. Y. Khrushchev, and I. Bennion, Opt. Lett. **31**, 1603 (2006).
20. A. Wolf, A. Dostovalov, K. Bronnikov, and S. Babin, Opt. Express **27**, 13978 (2019).
21. M. Haque, K. K. C. Lee, S. Ho, L. A. Fernandes, and P. R. Herman, Lab Chip **14**, 3817 (2014).
22. J. R. Grenier, L. A. Fernandes, and P. R. Herman, Opt. Express **23**, 16760 (2015).
23. A. Rahnama, K. M. Aghdami, Y. H. Kim, and P. R. Herman, Adv. Funct. Mater. **1**, 2000026 (2020).
24. J. Han, Y. Zhang, C. Liao, Y. Jiang, Y. Wang, C. Lin, S. Liu, J. Wang, Z. Zhang, J. Zhou, and Y. Wang, Opt. Express **28**, 14263 (2020).
25. S. Pissadakis, Microelectron. Eng. **217**, 111105 (2019).
26. Y. Chen, Y. Lai, and M. W. O. Cheong, Appl. Opt. **55**, 5575 (2016).
27. P. S. Salter, M. J. Woolley, S. M. Morris, M. J. Booth, and J. A. J. Fells, Opt. Lett. **43**, 5993 (2018).
28. P. S. Westbrook, K. S. Feder, T. Kremp, T. F. Taunay, E. Monberg, J. Kelliher, R. Ortiz, K. Bradley, K. S. Abedin, D. Au, and G. Puc, in *Optical Fibers and Sensors for Medical Diagnostics and Treatment Applications XIV*, vol. 8938 (SPIE, 2014), pp. 88–94.
29. P. S. Westbrook, K. S. Feder, T. Kremp, E. M. Monberg, H. Wu, B. Zhu, L. Huang, D. A. Simoff, S. Shenk, V. A. Handerek, M. Karimi, A. Nkansah, and A. Yau, iScience **23**, 101137 (2020).
30. M. Wang, Y. Yang, S. Huang, J. Wu, K. Zhao, Y. Li, Z. Peng, R. Zou, H. Lan, P. R. Ohodnicki, P. Lu, M. P. Buric, B. Liu, Q. Yu, and K. P. Chen, Opt. Express **28**, 20225 (2020).
31. M. Wang, K. Zhao, J. Wu, Y. Li, Y. Yang, S. Huang, J. Zhao, T. Tweedle, D. Carpenter, G. Zheng, Q. Yu, and K. P. Chen, Int. J. Extrem. Manuf. **3**, 025401 (2021).
32. C. G. Askins, M. A. Putnam, G. M. Williams, and E. J. Friebele, Opt. Lett. **19**, 147 (1994).
33. H. Yu, W. Gao, X. Jiang, H. Guo, S. Jiang, and Y. Zheng, Materials **12**, 1263 (2019).
34. P. Ji, S.-S. Lee, Y.-E. Im, and Y. Choi, Opt. Lett. **44**, 610 (2019).
35. J.-P. Bérubé, R. Vallée, M. Bernier, O. Kosareva, N. Panov, V. Kandidov, and S. L. Chin, Opt. Express **18**, 1801 (2010).
36. J. Lapointe, J.-P. Bérubé, S. Pouliot, and R. Vallée, OSA Continuum **3**, 2851 (2020).
37. D. Tan, X. Sun, Z. Li, and J. Qiu, Opt. Lett. **47**, 4766 (2022).
38. C. Hnatovsky, D. Grobnic, and S. J. Mihailov, Opt. Express **25**, 14247 (2017).
39. E. Bélanger, J.-P. Bérubé, B. de Dorlodot, P. Marquet, and R. Vallée, Opt. Express **26**, 17498 (2018).
40. X. Xiao, B. Xu, X. Xu, B. Du, Z. Chen, C. Fu, C. Liao, J. He, and Y. Wang, Opt. Lett. **47**, 758 (2022).
41. P. S. Westbrook, K. S. Feder, R. M. Ortiz, T. Kremp, E. M. Monberg, H. Wu, D. A. Simoff, and S. Shenk, in *25th International Conference on Optical Fiber Sensors*, vol. 10323 (SPIE, 2017), pp. 1399–1402.
42. P. Lu, S. J. Mihailov, D. Coulas, H. Ding, and X. Bao, J. Lightwave Technol. **37**, 4697 (2019).
43. F. Monet, S. Loranger, V. Lambin-Iezzi, A. Drouin, S. Kadoury, and R. Kashyap, Opt. Express **27**, 13895 (2019).